

<https://doi.org/10.1038/s43247-024-01413-8>

Exceptional atmospheric conditions in June 2023 generated a northwest European marine heatwave which contributed to breaking land temperature records

Check for updates

Ségolène Berthou¹✉, Richard Renshaw², Tim Smyth^{3,4}, Jonathan Tinker¹, Jeremy P. Grist⁵, Juliane Uta Wihsgott³, Sam Jones⁶, Mark Inall⁶, Glenn Nolan⁷, Barbara Berx⁸, Alex Arnold¹, Lewis P. Blunn¹, Juan Manuel Castillo¹, Daniel Cotterill^{1,9}, Eoghan Daly⁷, Gareth Dow¹, Breogán Gómez¹, Vivian Fraser-Leonhardt¹, Joel J.-M. Hirschi⁵, Huw W. Lewis¹, Sana Mahmood^{1,9} & Mark Worsfold¹

The Northwest European shelf experienced unprecedented surface temperature anomalies in June 2023 (anomalies up to 5 °C locally, north of Ireland). Here, we show the shelf average underwent its longest recorded category II marine heatwave (16 days). With state-of-the-art observation and modelling capabilities, we show the marine heatwave developed quickly due to strong atmospheric forcing (high level of sunshine, weak winds, tropical air) and weak wave activity under anticyclonic weather regimes. Once formed, this shallow marine heatwave fed back on the weather: over the sea it reduced cloud cover and over land it contributed to breaking June mean temperature records and to enhanced convective rainfall through stronger, warmer and moister sea breezes. This marine heatwave was intensified by the last 20-year warming trend in sea surface temperatures. Such sea surface temperatures are projected to become commonplace by the middle of the century under a high greenhouse gas emission scenario.

Marine heatwaves (MHW) are prolonged (>5 days) anomalously high sea surface temperature (SST) events (SST >90th centile of its daily climatology)¹. They can have strong ecological and socioeconomic impacts, such as mass coral bleaching in tropical regions², biological regime shifts in temperate regions³ and enhanced coastal urban heat islands⁴. They tend to be shorter lived in mid-latitudes (10–15 days), given the large amplitude of the annual cycle and variability of the jet stream: large-scale atmospheric pressure anomalies precede anomalous ocean warming in these regions^{5,6}. Wind speed suppression is the most common factor (82%) in MHW formation globally, with a majority also having a decrease in latent heat loss for subtropical and middle to high latitudes⁷. The most intense MHWs tend to occur in summer because of a shallow mixed layer, weaker wind speeds and higher variability

in solar radiation^{6–8}. Given that the continental shelf is shallow (30–250 m)⁹, SSTs here are more sensitive to regional and local scale drivers¹⁰.

Anthropogenic climate change has substantially increased the likelihood of MHWs over the past few decades^{11,12}. Future projections show an increasing trend in the intensity, extension and duration of MHWs in all warming scenarios (RCP2.6 or RCP8.5), with the most extreme MHWs (1 in 100 year event) becoming frequent in RCP8.5 (1 in 4 year) by the middle of the century^{12,13}.

We investigate the regional marine heatwave which affected the northwest European shelf (NWS) in June 2023. This event was preceded by an anomalously warm subtropical North Atlantic, and then northwest Atlantic waters, from May 2023¹⁴. A Mediterranean MHW followed in July.

¹Met Office, Exeter, UK. ²Met Office Hadley Centre, Exeter, UK. ³Plymouth Marine Laboratory, Plymouth, UK. ⁴Exeter University, Exeter, UK. ⁵National Oceanography Centre, Southampton, UK. ⁶Scottish Association for Marine Science, Oban, UK. ⁷Marine Institute, Oranmore, Ireland. ⁸Marine Directorate Scottish Government, Aberdeen, UK. ⁹University of Bristol, Bristol, UK. ✉e-mail: segolene.berthou@metoffice.gov.uk

Globally, SSTs reached unprecedented levels in August 2023¹⁴. This article gathers observational and model evidence of the MHW over the NWS; investigates its origins and feedbacks on the weather and sets it within the context of a changing climate.

Results

Characteristics of the marine heatwave

SSTs soared in the Northwest European shelf (NWS) in June 2023. The National Oceanic and Atmospheric Administration (NOAA) declared a category IV MHW for parts of it on 17 June. We follow NOAA definition in this article, which is based on Hobday et al. (2018): Category IV means SSTs were greater than their average by four times their daily 90th centile deviation calculated over 1982–2012¹. The average over the whole NWS was +2.9 °C warmer than climatological June in the Operational Sea Surface Temperature and Sea Ice Analysis system (OSTIA^{15,16}), based on satellite observations (Fig. 1a). Given that the 90th centile over the shelf is +1 °C, +2.9 °C corresponds to a category II MHW (twice above 90th centile anomaly) that lasted for 16 days, which is unprecedented in the last 40 years (1982–2022, Fig. 1a). The rapidity of the MHW onset was also remarkable: NWS-averaged anomalies rose from category I to category II in just 6 days (10–16 June). With a rise of 2.4 °C in 7 days, this trend is the second highest in the OSTIA 40-year record (Fig. 1d). Seasonally stratifying regions of the NWS experienced the strongest surface warming compared to shallow,

tidally mixed parts of the shelf (Channel and Irish sea in Fig. 1c). During the peak week (19–26 June, SSTs locally showed +5 °C anomalies in the central North Sea and the Irish shelf, reaching category IV in a few coastal areas (Fig. 1c). The Irish shelf anomaly started earlier (end of May) than in the central North Sea (second week of June) (Fig. S1). The local peaks are confirmed by gliders, which recorded near-surface temperatures over 16 °C in the Rockall Trough (Fig. 2a) and in the western North Sea (Fig. 2e), +4 °C and +5 °C above climatology for this time of year, and +2 °C above the average peak SSTs in August for these areas. The gliders east of Orkney observed peak SSTs of 14.5–15 °C, 3.5–4 °C above OSTIA climatology (Fig. 2c). The Western Channel Observatory also provided information on the MHW in the context of its long observational record (>100 years at location E1 and 40 years at L4; Fig. 2g, h). These locations showed a category I MHW throughout June, with record high temperatures for June at L4 (17.9 °C), and temperatures near the envelope of maximum recorded temperatures for E1.

The glider observations also provide information about the depth of the anomaly (Fig. 2b, d, f). All the gliders show a shoaling of the surface mixed layer (SML) depth from the start of June, with an extremely shallow SML (below 10 m) from 10 to 20 June, which deepens to 10–20 m from 20 to 30 June. E1 shows a 15 m depth SML on 27 June, 10 m shallower than in 2022 (Fig. S5d, e) and CTD profiles in the Celtic Sea on 22–23 June also recorded 5–15 m shallow SML (Fig. S5f). In late June and July, the mixed

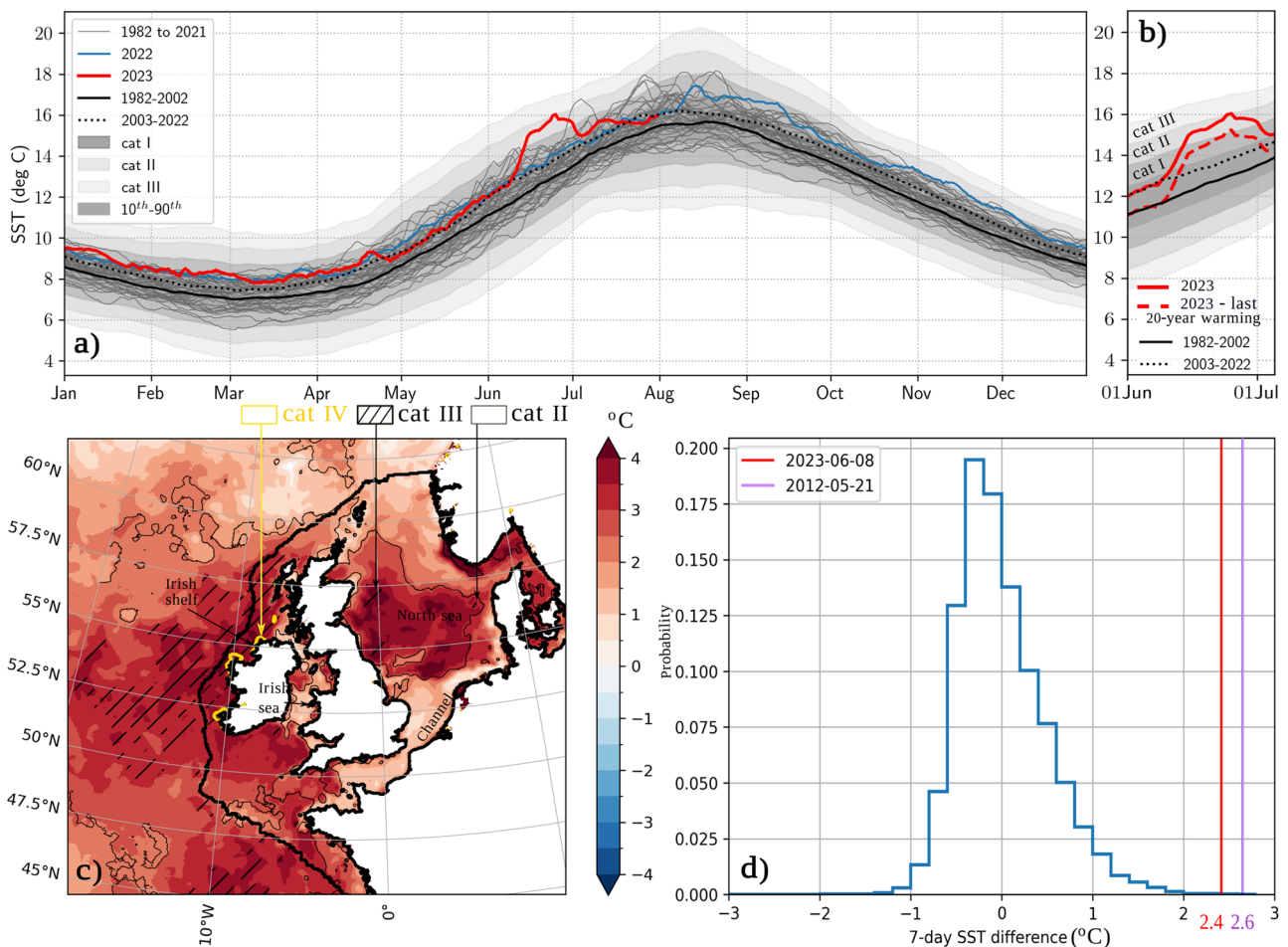


Fig. 1 | June 2023 marine heatwave characteristics from long-record satellite-based sea surface temperature dataset. a OSTIA SSTs for 1982–2023, mean climatologies (1982–2002 in full line and 2003–2022 in dotted line), 10th–90th centiles (anomalies smoothed with 31-day moving average), Shading: Category I, Category II, Category III marine heatwaves using Hobday et al.¹ averaged over the NWS (NWS=thick black contour in (c)). **b** Same as a, but zoomed over the MHW, dashed

red line is 2023–last 20-year trend **c** map of average OSTIA SST anomaly during peak week (19–25 June 2023) (relative to 1982–2012 mean), thin plain black contour: category II MHW, hashes: category III MHW, yellow contour: category IV MHW. **d** Normalised probability distribution of 7-day SST trends on the northwest European shelf—June 2023 maximum trend is in red (2.4 °C). It is the second highest trend after purple maximum trend (2.6 °C).

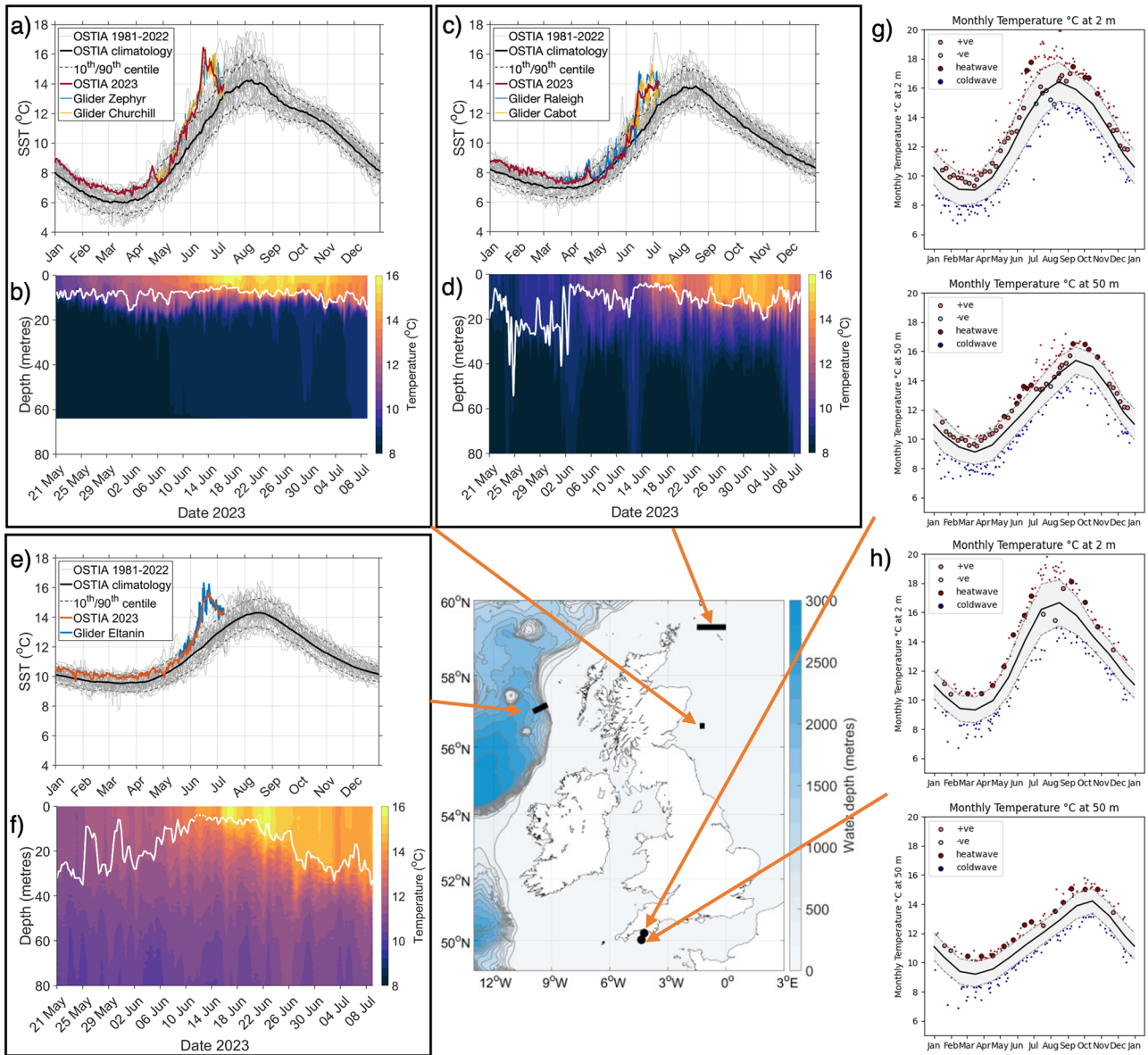


Fig. 2 | June 2023 marine heatwave characteristics from in-situ glider and Western Channel Observatory temperature observations: panel a, c, e near-surface (4 m) in-situ temperature observations, compared to closest OSTIA SST grid cells. Light grey lines show OSTIA daily SST between 1981 and 2023, heavy black line shows 1982–2010 daily mean (OSTIA) and black dashed line 10th/90th centile (OSTIA), panels b, d, f temperature profiles from gliders, white line shows SML depth. Panels g, h Monthly average temperature at 2 and 50 m depth (solid black line) for the Western Channel Observatory (WCO) time-series stations

at L4 (50°15.0'N; 4°13.0'W) and E1 (50°02.6'N; 4°22.5'W) together with the 90th and 10th centile (dashed line) region shaded in grey. Data for 2023 shown in large symbols with dark red shading depicting heatwave conditions, light red a positive anomaly, light blue a negative anomaly and dark blue cold wave conditions. Small symbols outside the centile range depict record temperature on a given day of year for years other than 2023. Averaging period for E1 is 1903–2023; L4 is 1988–2023. Sampling frequency at L4 is weekly (since 1988) and bi-weekly or monthly at E1 (since 2002).

layer depth increases (Figs. 2 and S2) and the anomalies reduce throughout the column, as also recorded for E1 and L4 at 50 m (Fig. 2g, h).

This June anomaly is additional to 2022 and early 2023 being 0.9 °C warmer than 1982–2012 climatology at the start of June across the NWS at the surface (Fig. 1b) and at depth (E1 and L4 in Fig. 2; EN4 profiles in Fig. S3b, c; and regional OCN_amm7_RAN reanalysis Fig. S4). This is consistent with the background 2003–2022 average being +0.9 °C warmer than 1982–2002 in June (Fig. 1b).

Origins of the marine heatwave

We first aim to isolate the role of ocean stratification pre-conditioning on the MHW. Most regions of the NWS experienced warmer than average temperatures throughout the water column in winter and spring

2023, prior to the June MHW development. The SML depth averaged over the NWS shows no anomalous behaviour in comparison to the past 22 years of the OCN_amm7_RAN reanalysis (Fig. S4). Seasonal stratification started in April and SML depth settled to ~20 m depth on average over the shelf around mid-May. Similarly, profiles in the Western Channel (E1, Fig. S5a, b) show a similar stratification in late May/early June of 2022 and 2023, suggesting no particularly strong or early stratification before the MHW. Further to this, the Price–Weller–Pinkel (“PWP”) one-dimensional upper ocean mixed layer model¹⁷ initialised from an EN4 profile close to where glider *Eltanin* (57 N 13 W) was operating and driven by ERA5 supported this finding (Fig. S2). Figure S6 (EN4 analysis) further supports the limited impact of salinity on June stratification¹⁸.

To further test this hypothesis, we applied a high resolution regional coupled model (UKC3¹⁷) to test whether the MHW would have developed across the NWS given the same atmospheric forcing but initialised from different ocean states representative of conditions in preceding years (Fig. S7). Results show that all simulations consistently develop the MHW, confirming little effect of ocean pre-conditioning and advection of Atlantic waters. Ocean pre-conditioning is therefore of secondary importance compared to atmospheric forcing.

Indeed, June 2023 was the sunniest June since 1957 over the United Kingdom¹⁹. ERA5 monthly mean net shortwave radiation confirms June 2023 was unusually sunny over the NWS as a whole (Fig. S8a). Latent heat fluxes were also lower than average (Fig. S8d). June ocean wave activity was the lowest recorded over the shelf in the last 40 years according to the NWS regional wave reanalysis WAVamm15_RAN (Fig. S9a, c), linked with both local (North Sea/NWS) and remote (North Atlantic) weak winds (Fig. S9d).

Figure 3 shows six stages of the MHW evolution, using output from km-scale coupled simulations (CPL, see Methods and note Section 2 in Supplementary material shows CPL simulations are of good quality compared to observations). We use the standard weather regime classification over Northwest Europe²⁰ to describe the weather situation (top row, Fig. 3). Stage 1 in the first week of June shows slow warming, with a high pressure system centred over the British Isles (weather regimes (WR) 25, 6, 9), very

high solar radiation (over 600 W m^{-2}) and low wind speeds (Fig. S10), which shoaled the SML by about 4 m. Stage 2 shows a warming hiatus on the 6–9 June, with a low-pressure system centred over the Azores, bringing windier conditions but also warm and moist tropical air over the NWS (Fig. S10). Stage 3 between the 10 and 17 June sees the strongest warming trend. High-pressure moved to Scandinavia (WR 5) and another low-pressure system over the mid-Atlantic maintained a weak flow of tropical air over the UK (WR 16). That week showed a combination of (i) high solar radiation with long hours of sunshine near the summer solstice (Fig. 3d); (ii) warm and moist air reducing sensible and latent heat fluxes and longwave radiative cooling (night-time cooling reduced to 50 W m^{-2} , Fig. S3e, Fig. S10); (iii) very weak winds (Fig. S10) and; (iv) neap tides (contributed to $+0.05 \text{ }^\circ\text{C}$ by shoaling the SML by 1 m compared to spring tides (Fig. S10)). The combination of (i), (iii) and (iv) shoaled the SML to less than 10 m and contributed to large shortwave radiative heating (SW) of the SML by $+10.0 \text{ }^\circ\text{C}$ over phases 1–3, only partially compensated by diurnal and tidal entrainment ($-2.7 \text{ }^\circ\text{C}$), longwave radiative cooling (LW, $-3.0 \text{ }^\circ\text{C}$), and weak latent (LH) and sensible (SH) cooling ($-1.6 \text{ }^\circ\text{C}$, Fig. 3d). The total surface heat fluxes contribution to SST trend in stages 1–3 was enhanced by 85% by shallowing of the SML (from $2.9 \text{ }^\circ\text{C}$ to $5.5 \text{ }^\circ\text{C}$, not shown). Figure 3d shows as an example that SW contribution would have been $5.7 \text{ }^\circ\text{C}$ instead of $10.0 \text{ }^\circ\text{C}$ if the SML had not shoaled (difference between SW term

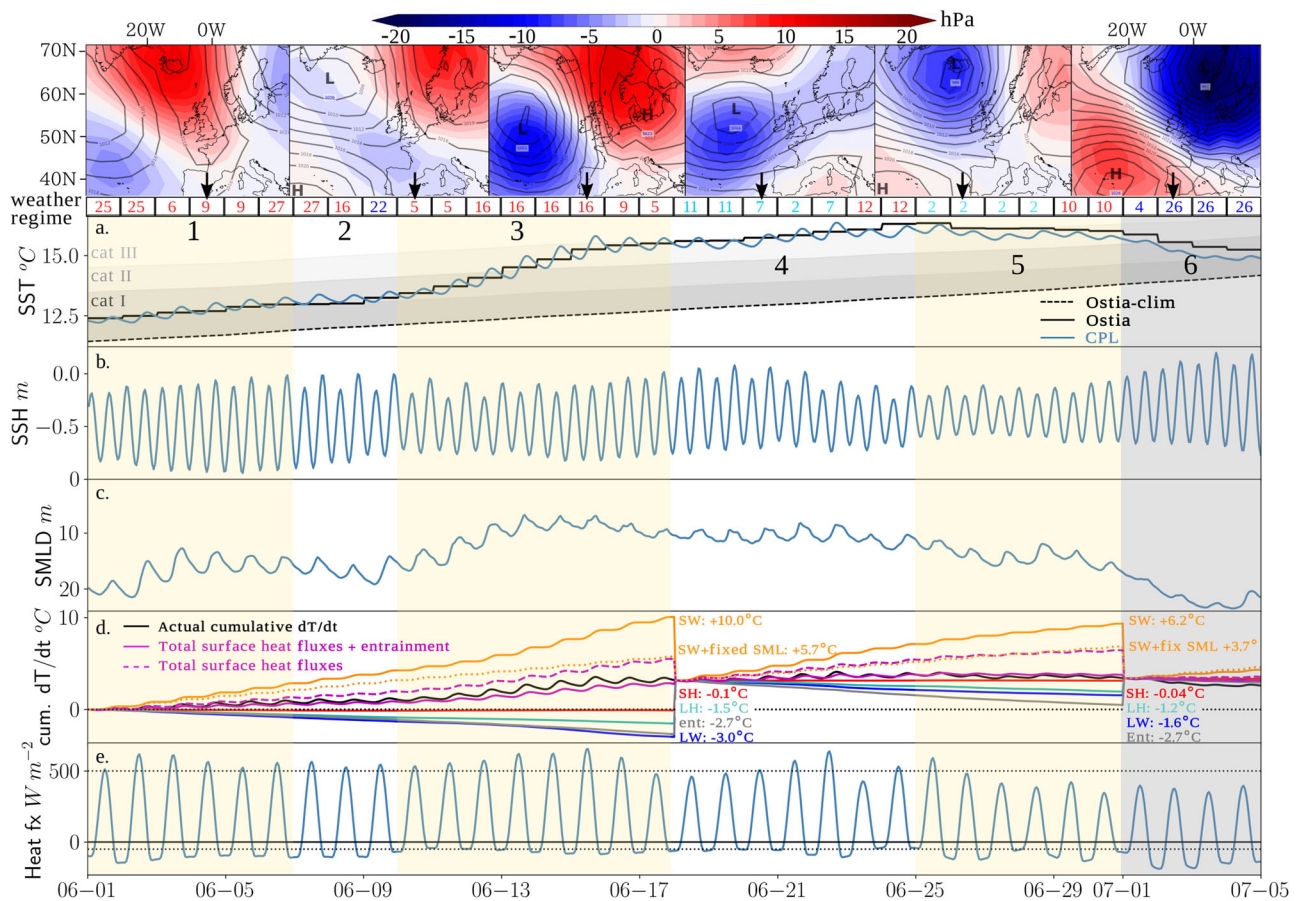


Fig. 3 | Atmospheric and oceanic states during the marine heatwave from high-resolution coupled simulations. Top row: table with numbers: weather regimes based on 30 clusters using Neal et al.⁴⁵, red means anticyclonic component over NWS, light blue cyclonic with weak circulation, dark blue strong cyclonic circulation. Weather regimes 9, 5, 16, 7, 2, 26 illustrated at the top (colour shading: mean sea level pressure (MSLP) anomalies (hPa) and MSLP mean values plotted in contours (2 hPa intervals)). Other rows: averages over the Northwest European Shelf (NWS) of: **a** Sea surface temperature ($^\circ\text{C}$) from OSTIA, OSTIA 1982–2012 climatology (Ostia-clim) and the coupled simulation CPL, **b** sea surface height (m)—anomaly from reference geoid, the amplitude of the variations show the tidal amplitude,

c surface mixed layer depth (de Boyer Montégut²² density calculation using $0.2 \text{ }^\circ\text{C}$ gradient and 3 m reference level) (m) **d** cumulative temperature trend from shortwave radiative (SW, yellow), longwave radiative (LW, blue), sensible (SH, red) and latent (LH, cyan) heat fluxes, from entrainment (deepening of the mixed layer, grey), SW + LW + SH + LH in dashed magenta and same terms + entrainment in magenta (Eq. 1 in Methods). Also added is SW calculated with SML depth from June 1st (fixed) in yellow dotted line. Black is the actual cumulative trend. Budget is reset to cumulated dT/dt at the start of phase 4 and 6. **e** hourly total heat flux into the ocean (SW + LW + SH + LH).

calculated with actual SML depth and SW term calculated with fixed SML depth from June 1st).

Figure 4 shows the spatial distribution of the SW, LW, LH and entrainment terms of the mixed layer heat budget (Eq. 1) cumulated over phases 1–3, as well as the SML depth at the start (June 1st) and the end (June 17th). Figure 4a shows the heterogeneity of the SML over the NWS on June 1st, with areas permanently mixed by tidal currents (Channel, Irish Sea) showing weak SST trends for all the terms. These areas keep a deep SML from the 1st to the 17th. In the rest of the domain, SML becomes shallower than 10 m on June 17th, meaning that some areas such as the Celtic Sea experienced a shallowing of the SML by about 30 m. The heat budget terms are largest in the areas where the SML was shallower from the start, mostly over the NWS and adjacent areas. The entrainment terms is also largest on the NWS and adjacent areas, where tidal energy dissipation enhances vertical mixing.

During stages 4 and 5, less strong shortwave influx (Fig. S3e) still results in +6 °C tendency (Fig. Sd) because of the shallow SML (Figs. 3c and 4d) but entrainment, latent heat and longwave radiative fluxes compensate it: the MHW is stable (Fig. 3d). Indeed, stage 4 saw the high-pressure system move south of the British Isles and most of NWS experienced weakly cyclonic conditions. Winds remained weak but solar heating was reduced due to clouds associated with weakly cyclonic regimes (WR 2, 7, 11, Fig. 3e, Fig. S10). The shallow mixed layer and persistent weak winds meant the heat remained trapped near the ocean surface, although spring tides started to deepen the mixed layer (by 2 m, Fig. S11). Stage 5 saw windier conditions, cloudier skies (WR 2), the SML deepened by 5 m but neap tide prevented an extra 1.5 m deepening and 0.1 °C cooling, Figure. S11). The surface anomaly remained until the start of July, when a low-pressure centre (WR 26) swept through with high wind speeds (10 m s⁻¹ averaged over NWS), both reducing and mixing the surface anomaly through the water column depth (Fig. 3c, d, S12). The high-pressure centre moved over central Europe in

July, and unsettled weather in July and early August brought SST and whole ocean heat content closer to average (Fig. 1a, E1 & L4 in Fig. 2, Fig. S12).

Feedbacks on the weather

Under persistent anticyclonic conditions, slow-moving air accumulates heat and moisture from the sea before being advected over land²¹. To assess the local atmospheric response to the MHW, Fig. 5 shows the difference between two 31-day duration high resolution regional weather simulations. One uses the observed daily SST during June 2023 as a lower boundary condition (labelled ATM_{ostia}) and the other uses a climatological SST (ATM_{clim}; shown in Fig. 3). Once the MHW is well established, its impact on the near-surface air temperature over the British Isles averages +1.1 °C during the last two weeks of June (stages 4 and 5). Figure 5c shows spatial anomalies to be especially strong in Scotland, Ireland, Wales, southwest England, Brittany and Denmark. Southeast England, northern France and the Netherlands show weaker warming because the SST anomaly in the Channel is relatively reduced (+1 °C) due to strong tidal mixing in this shallow area (Fig. 4d), which prevents a near-surface build-up of heat. During stage 4, the anomalous air temperature peaks at 16:00 UTC up to +1.5 °C on three days: 19, 21 and 23 of June (Fig. 5a). These peaks are associated with sea breezes, evident by stronger-than-usual diurnal peaks in land-average 10 m wind speeds (Fig. 5b).

Interestingly, winds are increased over land by the MHW during stage 4 (Fig. 5b), which is counter-intuitive given the land-sea contrast is reduced in the simulations with MHW (Fig. S13a). The sea breezes are driven by such a strong land-sea temperature gradient (5–10 °C) that their strength is not reduced by a –2 °C difference in the gradient (Fig. S13a). Instead, winds are increased over the ocean through a deeper boundary layer which brings more momentum near the surface (Fig. S14). This momentum increase over the sea is propagated over land by the sea breezes and reinforces them.

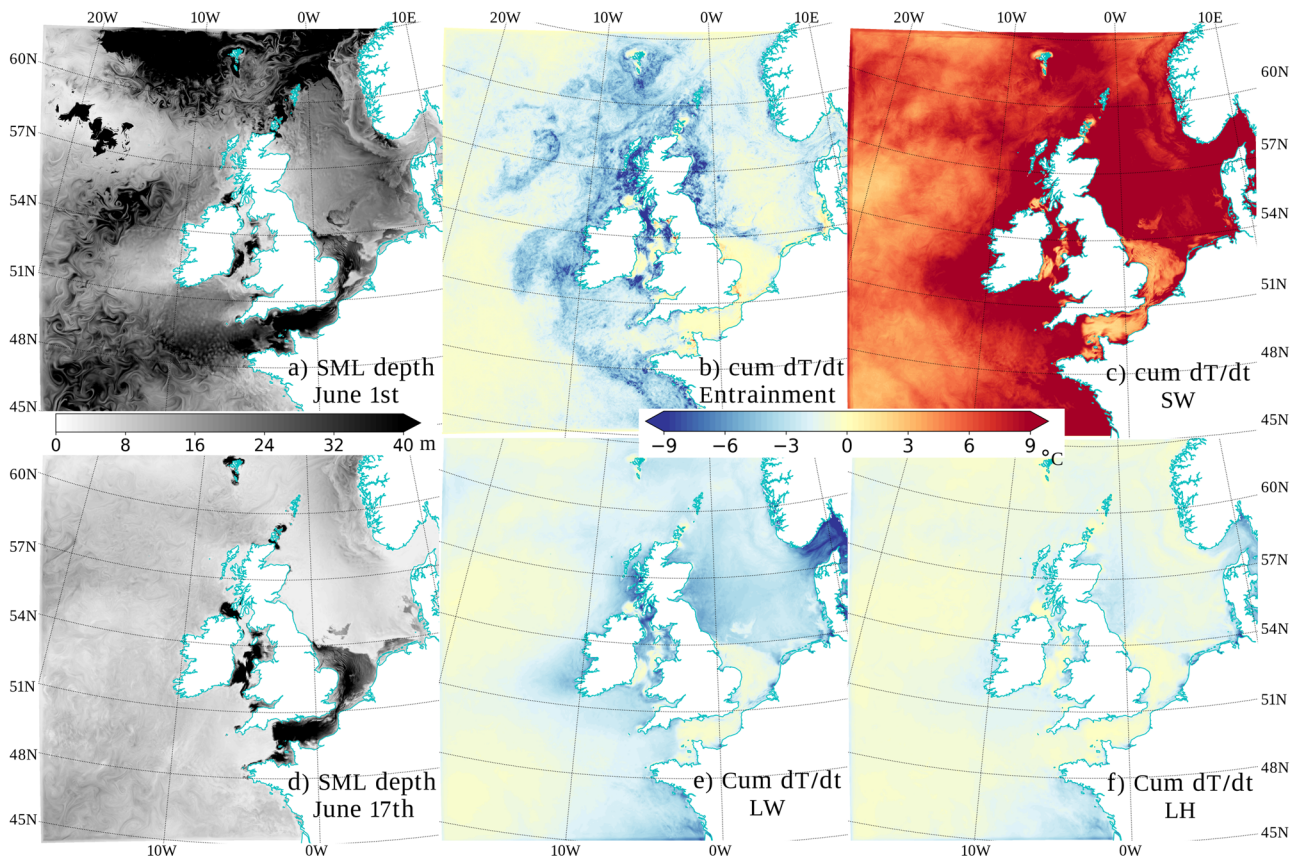


Fig. 4 | Surface mixed layer depth and mixed layer heat budget terms during the build-up phases (1–3) of the MHW from June 1st to June 17th in CPL. a SML depth on June 1st, **d** SML depth on June 17th **b** cumulative SST trend (1–17 June)

from entrainment at the bottom of the surface mixed layer, **c** from shortwave radiative flux, **e** from longwave radiative flux, **f** from latent heat flux. Note sensible heat flux not shown as tendencies are negligible compared to the other terms.

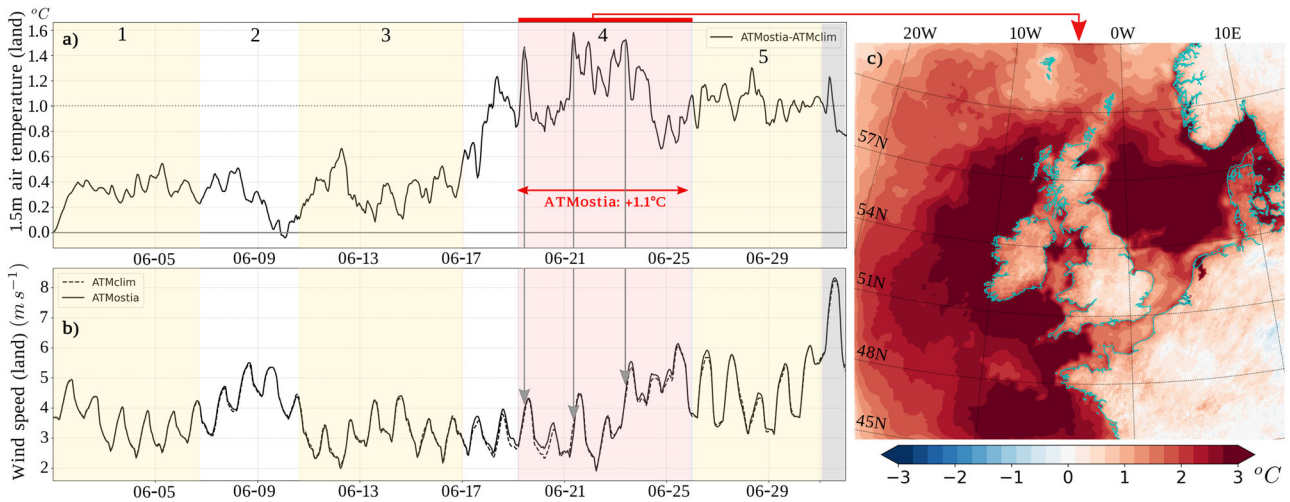


Fig. 5 | Effects of the marine heatwave on near-surface temperature and wind over land. **a** 1.5 m air temperature difference averaged over the British Isles between a regional atmospheric simulation with the observed marine heatwave (ATMostia, with OSTIA SSTs) and without (ATMclim, with climatological OSTIA SSTs). **b** Wind averaged over the British Isles in both simulations (ATMostia in full line and ATMclim in dashed line). **c** Map of 1.5 m air-temperature differences (ATMostia–ATMclim) averaged from 19 to 25 June (red area on **a**, **b**).

Higher humidity air is then advected over land (7% increase, Fig. S13b) and precipitation is increased by 23% over the British Isles because of the MHW during stage 4 (Fig. S13c). Precipitation during the week of 19 June is mostly convective and associated with convergence over land. On 21 June, a sea-breeze day, the probability of rainfall in England, Wales and Ireland was generally increased by the MHW, and convective events associated with sea breeze convergence in the English southwest peninsula would likely not have happened without the build-up of high SSTs over the preceding 2 weeks (Fig. S15).

The MHW increased temperature and precipitation over land, through advection of near-surface air temperature and moisture anomalies by sea breezes. Now, we demonstrate that the MHW generated daytime positive feedback on the weather over the sea (Fig. 6). Indeed, in stage 4, cloud cover was 15% lower over the shelf (Fig. 6a) in ATMostia compared to ATMclim, linked with a higher boundary layer height with warmer SSTs (Fig. S14). This increased the shortwave radiative heat flux into the ocean by 11% during stage 4 (up to 78 W m^{-2} , Fig. 5b). The reduced cloud cover is shown for 20 June at 15:00 UTC (Fig. 6c), with the probability of low-cloud cover exceeding 37.5% in an 18-member ensemble (ATMostia_ens) strongly reduced over the sea when compared with ATMclim_ens. Satellite data showed no low-level clouds southwest of the domain, in agreement with ATMostia (not shown). All the other heat fluxes (LW, SH, LH) tended to cool the ocean more with the MHW than without, due to raised SSTs and winds (negative feedback). However, the increased shortwave (SW) radiation by 11% counteracted the increased cooling by LW, SH and LH (Fig. 6b): the negative feedback was only 4% during stage 4, compared to 15% during stage 5. The positive SW feedback increased the temperature anomalies by 0.4°C during phase 4 (calculated using the SML heat budget in Eq. 1, see Methods). Without this positive feedback, the SST would have stayed stable, it would not have increased by a further 0.4°C during stage 4.

Marine heatwave in a changing climate

Finally, we investigate whether the June 2023 MHW over the NWS is part of a trend and quantify its projected future frequency. Figure 7a–c shows the warm and cold sea surface anomalies for the Western Channel Observatory (WCO) stations and OSTIA averaged over the NWS. There is a clear trend towards fewer cold and more warm spells over the past 20 years for both E1 and OSTIA datasets, in agreement with a previous study for OSTIA²². All three datasets show a stronger shift in the last 8 years. Remarkably, the last 2 years have seen very few cold spells in the WCO and none for the whole NWS. This coincides with the disappearance of the northeastern Atlantic

“cold blob” of 2015–2021²³ (Fig. S3a). The additional $+0.9^\circ\text{C}$ background warming anomaly for June from the last 20 years lifted the MHW intensity up to category II instead of category I for 16 days (Fig. 1a). However, the anticyclonic weather regime period linked with the build-up of the MHW is likely coming from weather variability or potentially teleconnections with a transition from La Niña to El Niño²⁴; no recent trend in WRs 5, 6, 9 and 16 is clearly linked with climate change²⁵.

To assess how this MHW compares to future projections, we make use of the NWS future projections²⁶: a 12-member regional ocean downscaling of the Hadley Centre Perturbed Parameter Ensemble (PPE²⁷). This NWS PPE ensemble uses a high-end Representative Concentration Pathway (RCP8.5) with a high climate sensitivity global climate model. In this global ensemble, global mean temperatures reach $+1.9^\circ\text{C}$ ($1.7\text{--}2.2^\circ\text{C}$) by 2040–2059 compared to 2000–2019. The daily mean SST increase over the NWS in Fig. 7d suggests that temperatures observed during the 2023 June MHW would be considered a small warm anomaly ($+0.3^\circ\text{C}$) by 2040–2059, an average month by 2050–2069, and would be considered a cold spell by the end of the century (2079–2098) (Fig. S16). Using the Hobday MHWs analysis¹ on the NWS PPE, we find a rise of the percentage of the year experiencing a MHW from 8% in 2000–2019 to 66% in 2040–2059 and finally 93% by the last 20 years of the century (Figs. S17–20, Fig. S21c, Table S1). By 2079–2098, 39% of the NWS experience MHWs more than 95% of the time (Fig. S20, Table S1). The average temperature above the 90th centile threshold (relative to 2000–2019) is $+0.44^\circ\text{C}$ (2000–2019), $+0.89^\circ\text{C}$ (2040–2059) and $+2.11^\circ\text{C}$ (2079–2098) (Fig. S20f). We note that summer SSTs increase more than winter SSTs, making the early summer (May/June) warming trends stronger. The weather regimes (WR) associated with the build-up (phases 1–3) and stationarity (phases 4–5) of this MHW are projected to slightly increase in frequency in summer by the end of the century by about 0.25% and 0.6% respectively, while WR associated with its breakdown (phase 6) should decrease slightly (-0.35%) (Fig. S21).

Summary and discussion

The June 2023 MHW which affected the northwest European shelf was unprecedented in terms of intensity and duration. It started in late May over the eastern Atlantic and in early June over the shelf itself. Persistent anticyclonic weather patterns with weak winds and long hours of sunshine were responsible for first increasing the ocean stratification and then SSTs in the first half of June. In the second week of June, warm, moist air advected over the shelf by a remote low-pressure system additionally

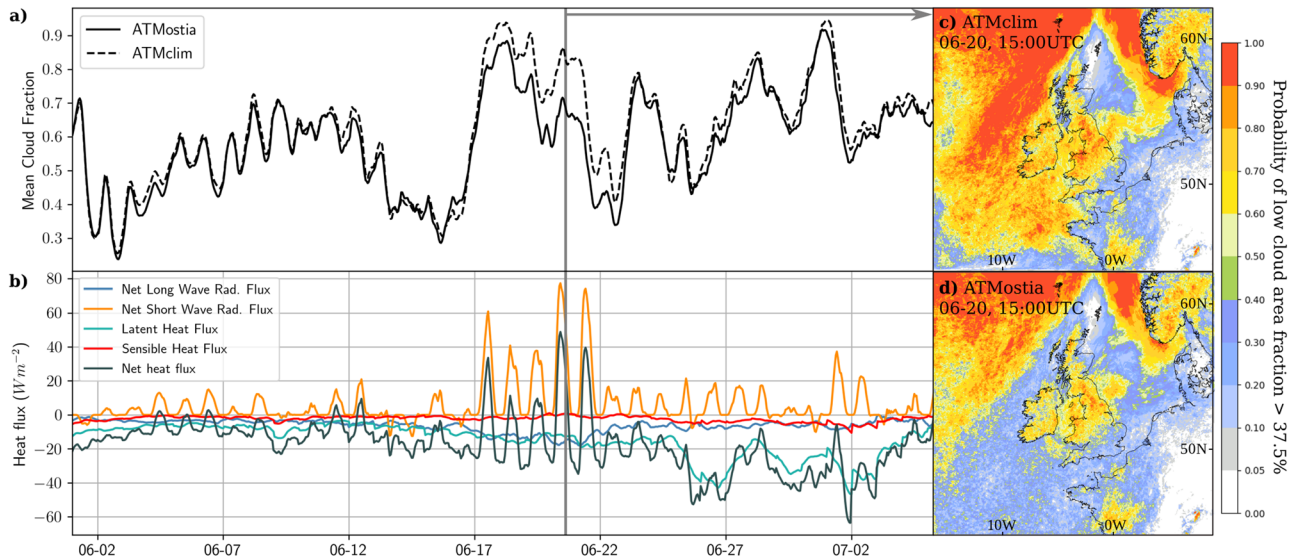


Fig. 6 | Positive cloud feedback over the ocean. **a** Mean cloud fraction over sea (averaged over the whole atmospheric column and over the northwest shelf) in the regional atmospheric simulation with MHW (ATMostia in full line) and without (ATMclim in dashed line). **b** Difference in heat flux (positive indicates more heat flux

into the ocean) between ATMostia and ATMclim: net heat flux (dark green), SH (red), LH (sea blue), LW (blue), SW (yellow). **c** Probability of low cloud cover fraction >37.5% for 20 June 20 at 15:00UTC (grey line in **a**, **b**) in an ensemble of regional ATMclim started on 19 June. **d** Same as **c** but with ATMostia.

reduced ocean cooling. This led to very rapid warming (2nd fastest 7-day trend recorded over the last 40 years). Once established, the MHW lasted for another two weeks: although sunshine was reduced in weakly cyclonic conditions, the winds and waves were still weak and the SML remained extremely shallow: SW heating still compensated all the other cooling processes. SW radiation was reinforced by 11% by a reduction in low-level cloud due to the MHW itself, and the last week of June saw continued weak winds and particularly neap tides, both preventing SML deepening.

We have demonstrated that the MHW had a strong impact on the weather over land: the United Kingdom broke its record June monthly temperature by +0.9 °C, of which we quantify that 0.6 °C came from the feedback of the MHW. During the peak week of the MHW, the British Isles were 1.1 °C warmer and experienced 23% more rainfall, although water vapour only increased by 7%/°C, in line with the Clausius-Clapeyron relationship. We suggest that continued studies of regional response of rainfall to MHWs may help constrain regional water cycle response to climate change.

The extreme 7-day trend in SST which started the MHW is a good example of a situation when regional numerical weather prediction (NWP) quality is reduced by keeping a fixed SST over 7-days²⁸, which is the default practice in many forecasting centres. The Met Office recently implemented a time-varying SST in its weather forecast thanks to its marine forecasting system²⁸. Figure S22 shows benefits of this system even for short 36 h forecasts during the MHW.

The MHW intensity would have reached category I instead of II without the warming trend from the last 20 years. Its longevity however is most likely linked with climate variability. We suggest weather regimes 5, 6, 9, 16 should be monitored in long-range weather forecasting to help forecast MHWs over the NWS. In RCP8.5 projections, the SSTs experienced during this MHW are to become average past mid-century: impact studies on ecosystem health and its resilience to MHWs are needed.

The positive feedback of MHW on low-level cloud cover, serving to maintain extreme conditions, is further demonstration of the close coupling between the ocean and atmosphere across scales from basin to coastal scale. The availability of regional coupled modelling systems offers novel ways to explore these interactions and run counter-factual experiments such as our “climatological SST” summer. Given these

strong influences, it is important that regional climate change projections should move towards coupled model approaches, in addition to advancing their use to underpin short-range hazard prediction in several operational centres^{17,29}.

Methods

Climate analysis methodology (Fig. 6)

Our climate analysis was based on OCN_amm7_proj²⁶. Full details of our methodology are available in the Supplementary material, Section 1. Briefly, we assessed how the regional SST will change, and compared to the OCN_amm7_RAN in Fig. 6d (and Fig. S14). We then developed a two-dimensional version of the Hobday MHW method and applied it to the OCN_amm7_proj, and assessed changes in the average and total duration of MHWs with the 20-year period, and their average and total intensity (Figs. S23–25).

Surface mixed layer heat budget (Fig. 3)

We considered SML as fully mixed and used a bulk formula for the SML heat budget³⁰, with an entrainment term³¹.

$$\frac{dT(t)}{dt} = \frac{Q_{SW} \left(1 - (1 - 0.58)e^{-\frac{h(t)}{3}} \right)}{\rho C_p h(t)} + \frac{Q_{LH} + Q_{SH} + Q_{LW}}{\rho C_p h(t)} - \epsilon \frac{T(t-1) - T_{dh}(t-1)}{h(t)} \frac{dh(t)}{dt} + R \quad (1)$$

$T(t)$ is temperature averaged over the SML at hour t , Q_{SW} is SW flux at the surface, $(1 - 0.58)Q_{SW}e^{-\frac{h(t)}{3}}$ is shortwave flux at the bottom of the SML, according to the RGB NEMO parameterisation used in CPL, $Q_{LH} + Q_{SH} + Q_{LW}$ are latent heat, sensible heat and longwave radiative heat flux respectively, ρ is density (1027), C_p is heat capacity of water (3850 J kg⁻¹ °C⁻¹), h is SML depth (m), calculated by de Boyer Montégut³² (3 m reference level, 0.2 °C temperature (density equivalent) gradient), $T_{dh}(t-1)$ is the temperature averaged over the entrained layer ($h(t-1)$ to $h(t)$) (°C), ϵ is a Heaviside function: 0 when $\frac{dh}{dt} < 0$ and 1 when $\frac{dh}{dt} > 0$. $\frac{dh}{dt}$ is the change in SML depth from $t-1$ to t . R is the remaining terms (including advection). We calculated each term at every grid point on an hourly basis and averaged

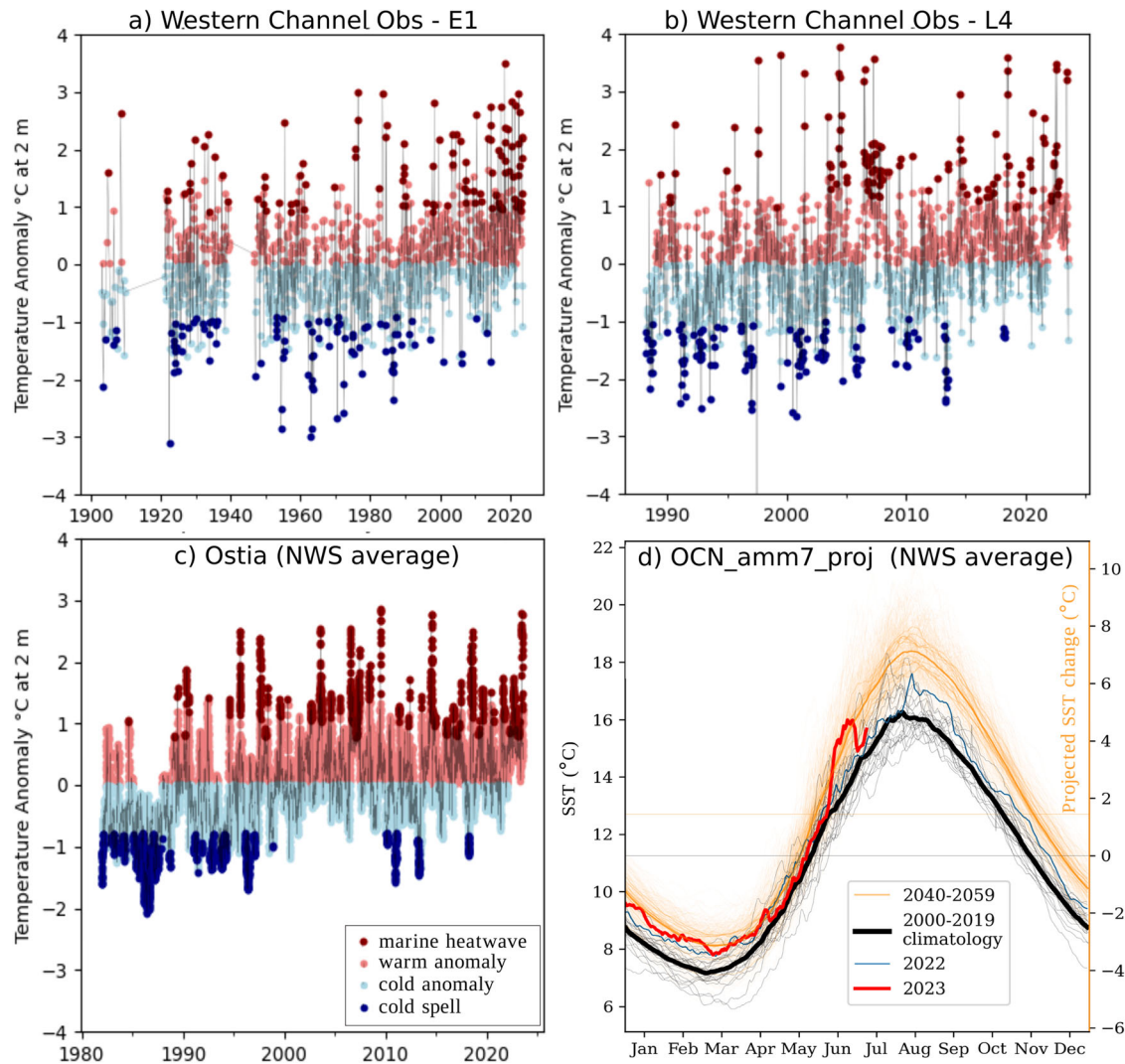


Fig. 7 | Observed and projected trends in sea surface temperatures. **a** 1903–Aug 2023 2 m depth temperature anomaly timeseries at E1, **b** 1988–Aug 2023 2 m depth temperature anomaly timeseries at L4 (see Fig. 2 for location). Light red circles are positive anomalies, dark red circles represent heatwave conditions (>90th centile); Light blue circles are negative anomalies, dark blue circles represent cold spell

conditions (<10th centile). **c** 1982–2023 OSTIA foundation SST timeseries averaged over the NWS. **d** Annual cycle of SSTs averaged across the NWS: grey 2000–2019 OCN_amm7_RAN reanalysis, orange future changes from NWS PPE projections (2040–2059). Bold line is the daily average. Left axis actual value, right axis shows SST difference with present-day. Blue line is 2022, red line 2023.

them over the NWS. Note we added a condition that $\frac{dh}{dt} < 2 \text{ m h}^{-1}$ to avoid large jumps in the SML depth diagnostic.

Data availability

Gliders (Fig. 2): Near-real time temperature data from three active ocean glider missions were used to investigate the water column structure prior to and during the MHW in June. In total, 5 vehicles were deployed consisting of one Seaglider in the Rockall Trough³³ (Ellett Array), two Slocum gliders (PELAGIO) east of the Firth of Forth and a further two Slocum gliders (MOGLi) east of Orkney, all performing continuous transects. All gliders were equipped with Seabird CT sails. Temperature observations from each glider were interpolated onto 6 hr time steps and a 1 m depth grid. The shallowest ‘good’ depth cell (4 m) was taken to represent the near-surface temperature time-series. The SML depth was defined at each time step as the depth at which the temperature deviated from the surface value by more than 0.2 °C. Glider data are available through the British Oceanographic Data Centre (https://linkedsystems.uk/erddap/files/Public_Glider_Data_0711/). *Western Channel Observatory*³⁴ (E1/L4) (Figs. 2 and 6): The depth resolved temperature time-series at the WCO is maintained by station L4

and E1 occupations on a weekly and bi-weekly (monthly in winter) basis by research vessel (RV) Plymouth Quest. The Conductivity Temperature Depth (CTD) profiles are binned into 0.25 m averages between the sub-surface and sea-floor (L4: 50 m; E1: 80 m). From the temperature series, a monthly mean and associated standard deviation has been calculated (L4: 1988–2023; E1: 1903–2023) and anomalies determined for 2 m and 50 m depths. The condition of heatwave (coldwave) was determined by 1.28× standard deviation (equivalent to 90th centile in a Gaussian distribution), which was necessarily interpolated onto a daily grid from the monthly values so that individual data samples could be accurately assessed as crossing these thresholds. Data available on doi:10.5281/zenodo.10892078. *EN4*³⁵ (Fig. S3): The EN.4.2.2 objective analyses which utilises the Gouretski and Reseghetti (2010)³⁶ XBT corrections and Gouretski and Cheng (2020)³⁷ MBT corrections were used in this work. *PWP*³⁸ (Fig. S2): We use the Price–Weller–Pinkel (“PWP”) one-dimensional upper ocean mixed layer model developed specifically for conditions of large diurnal solar radiance and demonstrated to have wide applicability and to out-perform more sophisticated mixing models³⁹. The PWP model was forced with ERA5 hourly fluxes (S.W., L.W., Latent, Sensible, east and west turbulent stresses and E–P), covering the years 1973–2023. The background vertical diffusivity

was set to $Kz = 2e - 5 m^2 s^{-1}$. The model was run with a vertical grid size of 1 m and a time step of one hour. Each of the 51 individual simulations (January to July of 1973 to 2023) was initialised using an Argo TS profile from Jan 2023 (57 N 13 W) to control for decadal ocean heat and salt content variation, thus isolating the influence of air/sea exchange on the seasonal development in each of the years and allowing for a comparative ocean response analysis between the years. OSTIA¹⁶ (Fig. 1): The Operational Sea Surface Temperature and Ice Analysis provides daily gap-free maps of Foundation Sea Surface Temperature at $0.05^\circ \times 0.05^\circ$ horizontal grid resolution in near real time, using in-situ and satellite data from both infra-red and microwave radiometers. <https://doi.org/10.48670/moi-00165>. Ocean reanalyses: OSTIA_CLIM¹⁶ (Fig. 1): Climate quality version of the OSTIA SST analysis, similar to the near real time product but produced in slower time using reprocessed, climate quality, in situ and satellite observations. We used the 1982–2012 daily average as reference climatology. <https://doi.org/10.48670/moi-00168>. Ocean model simulations (forecast or re-analysis): OCN_amm7_RAN¹⁰ (Fig. S4): 30-year (1993–2023) reanalysis from the Met Office NWS forecasting ocean assimilation model (NEMO) run on the AMM7 NWS domain, 7 km resolution, with tides. OCN_amm7_RAN assimilates satellite SST, and in situ temperature and salinity. <https://doi.org/10.48670/moi-00059>. OCN_amm7_proj²⁶ (Fig. 6, S16–20): An ensemble of physical marine climate projections using with the same model as OCN_amm7_RAN have recently been released. A HadGEM3-GC3.05 Perturbed Parameter Ensemble, run under the RCP8.5 scenario, was dynamically downscaled for the NWS with NEMO AMM7. The 12 ensemble members were run as transient simulations (from 1990 to 2098). The monthly mean data was released on the CEDA Archive <https://catalogue.ceda.ac.uk/>, <https://doi.org/10.5285/edf66239c70c426e9e9f19da1ac8ba87>. WAVamm15_RAN (Fig. S9): Wave hindcast using WAVEWATCH III for the North-West European Shelf with a two-tier Spherical Multiple Cell grid mesh (3 and 1.5 km cells). The model is forced by lateral boundary conditions from a Met Office Global wave hindcast. The atmospheric forcing is given by ERA5. <https://doi.org/10.48670/moi-00060>. Coupled model simulations: CPL (Figs. 3 and S7): Atmosphere-ocean-wave coupled simulation using the updated UKC3 coupled system¹⁷. It couples the Met Office Unified Model & land surface (JULES) using Regional Atmosphere and Land 2 (RAL2⁴¹) scientific configuration, currently operational at the Met Office, with a shelf-sea ocean (NEMO, Atlantic Margin Model 1.5 km configuration, operational⁴²) and ocean surface waves WAVEWATCH III (operational), coupled together using OASIS3-MCT libraries. The simulations were started on June 1st from Met Office operational analyses and lateral boundary conditions (LBC). Evaluation of the coupled model is provided in Supplementary Material, Section 2 (Fig. S26–3). CPLics2020, CPLics2021, CPLics2022 (Fig. S7): Same as CPL but using initial conditions and LBCs for the ocean for June 2020, 2021, 2022 respectively. Atmospheric model simulations: ATMostia (Figs. 4 and 5): Same atmosphere and land as CPL above but its SST is OSTIA_2023 (run for a clean comparison with OSTIA_CLIM). ATMclim (Figs. 4 and 5): Same as above but SST is from OSTIA_CLIM averaged daily over 1982–2012. ATMostia_ens and ATMclim_ens (Figs. 5 and S15): Same set-up as ATMostia but run as an 18-member ensemble forecast started on June 19th for a 5-day forecast⁴³. An ensemble is best to assess impact of SST on hourly precipitation or cloud features, as changes in a single hindcast member for such a short window would be affected by internal variability. The data underlying the main figures is provided here: 10.5281/zenodo.10892078. Atmospheric reanalysis: ERA5³⁸ (Fig. S8): Global atmospheric reanalysis produced under the Copernicus Climate Change Service (C3S)⁴⁴. Annual time series of SST and surface heat flux components with monthly data averaged over the NW European shelf were plotted for 1980–2023. <https://doi.org/10.24381/cds.143582cf>

Code availability

The code underlying the main figures is provided here <https://doi.org/10.5281/zenodo.10892078>.

Received: 19 February 2024; Accepted: 23 April 2024;

Published online: 30 May 2024

References

- Hobday, A. J. et al. Categorizing and naming marine heatwaves. *Oceanography* **31**, 162–173 (2018).
- Shlesinger, T. & van Woeseik, R. Oceanic differences in coral-bleaching responses to marine heatwaves. *Sci. Tot. Env.* **871**, 162113 (2023).
- Wernberg, T. et al. Climate-driven regime shift of a temperate marine ecosystem. *Science (1979)* **353**, 169–172 (2016).
- Hu, L. A global assessment of coastal marine heatwaves and their relation with coastal urban thermal changes. *Geophys. Res. Lett.* **48**, e2021GL093260 (2021).
- Holbrook, N. J. et al. A global assessment of marine heatwaves and their drivers. *Nat. Commun.* **10**, 2624 (2019).
- Oliver, E. C. J. et al. Marine heatwaves. *Ann. Rev. Mar. Sci.* **13**, 313–342 (2021).
- Sen Gupta, A. et al. Drivers and impacts of the most extreme marine heatwaves events. *Sci. Rep.* **10**, 19359 (2020).
- Vogt, L., Burger, F. A., Griffies, S. M. & Frölicher, T. L. Local drivers of marine heatwaves: a global analysis with an earth system model. *Front. Clim.* **4** (2022).
- Huthnance, J. et al. Ocean shelf exchange, NW European shelf seas: measurements, estimates and comparisons. *Prog. Oceanogr.* **202**, 102760 (2022).
- Schlegel, R. W., Oliver, E. C. J., Wernberg, T. & Smit, A. J. Nearshore and offshore co-occurrence of marine heatwaves and cold-spells. *Prog. Oceanogr.* **151**, 189–205 (2017).
- Oliver, E. C. J. et al. Longer and more frequent marine heatwaves over the past century. *Nat. Commun.* **9**, 1324 (2018).
- IPCC. Extremes, Abrupt Changes and Managing Risks. *The Ocean and Cryosphere in a Changing Climate* 589–656 <https://doi.org/10.1017/9781009157964.014> (2022).
- Frölicher, T. L., Fischer, E. M. & Gruber, N. Marine heatwaves under global warming. *Nature* **560**, 360–364 (2018).
- Kuhlbrodt, T., Swaminathan, R., Ceppi, P. & Wilder, T. A glimpse into the future: the 2023 ocean temperature and sea-ice extremes in the context of longer-term climate change. *Bull. Am. Meteorol. Soc.* <https://doi.org/10.1175/BAMS-D-23-0209.1> (2024).
- Donlon, C. et al. The Operational Sea Surface Temperature and Sea Ice Analysis (OSTIA) system. *Remote Sens. Environ.* **116**, 140–158 (2012).
- Good, S. et al. The current configuration of the OSTIA system for operational production of foundation sea surface temperature and ice concentration analyses. *Remote Sens. (Basel)* **12**, 720 (2020).
- Lewis, H. W. et al. The UKC3 regional coupled environmental prediction system. *Geosci. Model. Dev.* **12**, 2357–2400 (2019).
- Jardine, J. E. et al. Rain triggers seasonal stratification in a temperate shelf sea. *Nat. Commun.* **14**, 3182 (2023).
- Met Office. *June 2023 Monthly Weather Report*. https://www.metoffice.gov.uk/binaries/content/assets/metofficegovuk/pdf/weather/learn-about/uk-past-events/summaries/mwr_2023_06_for_print.pdf (2023).
- Neal, R., Fereday, D., Crocker, R. & Comer, R. E. A flexible approach to defining weather patterns and their application in weather forecasting over Europe. *Meteorol. Appl.* **23**, 389–400 (2016).
- Duffourg, F. & Ducrocq, V. Origin of the moisture feeding the Heavy Precipitating Systems over Southeastern France. *NHESS* **11**, 1163–1178 (2011).
- Peal, R., Worsfold, M. & Good, S. Comparing global trends in marine cold spells and marine heatwaves using reprocessed satellite data. *State Planet 1-osr7*, 3 (2023).
- Josey, S. A. & Marsh, R. Surface freshwater flux variability and recent freshening of the North Atlantic in the eastern subpolar gyre. *J. Geophys. Res.* **110**, C05008 (2005).

24. McKenna, M. & Karamperidou, C. The impacts of El Niño diversity on northern hemisphere atmospheric blocking. *Geophys. Res. Lett.* **50**, e2023GL104284 (2023).
25. Cotterill, D. F., Pope, J. O. & Stott, P. A. Future extension of the UK summer and its impact on autumn precipitation. *Clim. Dyn.* **60**, 1801–1814 (2023).
26. Tinker, J. et al. 21st century marine climate projections for the NW European Shelf Seas based on a Perturbed Parameter Ensemble. *EGUSphere* **2023**, 1–66 (2023).
27. Yamazaki, K. et al. A perturbed parameter ensemble of HadGEM3-GC3.05 coupled model projections: Part 2: global performance and future changes. *Clim. Dyn.* **56**, 3437–3471 (2021).
28. Mahmood, S. et al. The impact of time-varying sea surface temperature on UK regional atmosphere forecasts. *Meteorol. Appl.* **28**, e1983 (2021).
29. Sauvage, C., Lebeaupin Brossier, C. & Bouin, M.-N. Towards kilometer-scale ocean–atmosphere–wave coupled forecast: a case study on a Mediterranean heavy precipitation event. *Atmos. Chem. Phys.* **21**, 11857–11887 (2021).
30. Elzahaby, Y., Schaeffer, A., Roughan, M. & Delaux, S. Why the mixed layer depth matters when diagnosing marine heatwave drivers using a heat budget approach. *Front. Clim.* **4** (2022).
31. Kim, S.-B., Fukumori, I. & Lee, T. The closure of the ocean mixed layer temperature budget using level-coordinate model fields. *J. Atmos. Ocean Technol.* **23**, 840–853 (2006).
32. de Boyer Montégut, C., Madec, G., Fischer, A. S., Lazar, A. & Iudicone, D. Mixed layer depth over the global ocean: an examination of profile data and a profile-based climatology. *J. Geophys. Res.* **109**, C12003 (2004).
33. Fraser, N. J. et al. North Atlantic current and European slope current circulation in the rockall trough observed using moorings and gliders. *J. Geophys. Res. Oceans* **127**, e2022JC019291 (2022).
34. Smyth, T. J. et al. A broad spatio-temporal view of the Western English Channel observatory. *J. Plankton Res.* **32**, 585–601 (2010).
35. Good, S. A., Martin, M. J. & Rayner, N. A. EN4: quality controlled ocean temperature and salinity profiles and monthly objective analyses with uncertainty estimates. *J. Geophys. Res. Oceans* **118**, 6704–6716 (2013).
36. Gouretski, V. & Reseghetti, F. On depth and temperature biases in bathythermograph data: development of a new correction scheme based on analysis of global ocean database. *Deep-Sea Res.* <https://doi.org/10.1016/j.dsr.2010.03.011> (2010).
37. Gouretski, V. & Cheng, L. Correction for systematic errors in the global dataset of temperature profiles from mechanical bathythermographs. *J. Atmos. Ocean Technol.* **37**, 841–855 (2020).
38. Price, J. F., Weller, R. A. & Pinkel, R. Diurnal cycling: observations and models of the upper ocean response to diurnal heating, cooling, and wind mixing. *J. Geophys. Res. Oceans* **91**, 8411–8427 (1986).
39. Damerell, G. M. et al. A comparison of five surface mixed layer models with a year of observations in the North Atlantic. *Prog. Oceanogr.* **187**, 102316 (2020).
40. Renshaw, R., Wakelin, S. L., Mahdon, R., O’Dea, E. & Tinker, J. *Copernicus Marine Environment Monitoring Service Quality Information Document North West European Shelf Production Centre NORTHWESTSHELF_REANALYSIS_PHYS_004_009*. <http://marine.copernicus.eu/documents/QUID/CMEMS-NWS-QUID-004-009.pdf> (2019).
41. Bush, M. et al. The second Met Office Unified Model–JULES Regional Atmosphere and Land configuration, RAL2. *Geosci. Model. Dev.* **16**, 1713–1734 (2023).
42. Tonani, M. et al. The impact of a new high-resolution ocean model on the Met Office North-West European Shelf forecasting system. *Ocean Sci.* **15**, 1133–1158 (2019).
43. Gentile, E. S., Gray, S. L. & Lewis, H. W. The sensitivity of probabilistic convective-scale forecasts of an extratropical cyclone to atmosphere–ocean–wave coupling. *Q. J. R. Meteorol. Soc.* **148**, 685–710 (2022).
44. Hersbach, H. et al. The ERA5 global reanalysis. *Q. J. R. Meteorol. Soc.* **146**, 1999–2049 (2020).
45. Neal, R. Daily historical weather pattern classifications for the UK and surrounding European area (1950 to 2020). <https://doi.org/10.1594/PANGAEA.942896> (2022).

Acknowledgements

The Western Channel Observatory is funded by the UK Natural Environment Research Council (NERC), grant number NE/R015953/1. PELAgIO is part of the ‘The Ecological Consequences of Offshore Wind’ (ECOWind) programme, grant number NE/X00886X/1. JT, SB, AA, RR, DC were supported by the Met Office Hadley Centre Climate Programme funded by DSIT. This work also benefitted from funding from the UK government / DSIT Earth Observation Investment Package <https://www.gov.uk/government/publications/earth-observation-investment/projects-in-receipt-of-funding>. Ellett Array glider, SJ and MI were funded by NERC programmes CLASS NE/R015953/1 and OSNAP NE/K010700/1. We thank Ciaran O’Donnell and the crew of the RV Celtic Explorer who gathered the Marine Institute profiles. We thank the WesCon field campaign which triggered this analysis. The authors are grateful to the anonymous reviewers who helped improve the manuscript. © Crown Copyright, Met Office.

Author contributions

S.B. led the coupled & atmospheric experiments and coordinated/wrote the article, R.R. did the OSTIA & OCN_amm7_RAN data analysis, T.S. provided & analysed WCO data, J.T. ran and analysed the OCN_amm7_proj, J.G. provided EN4 & ERA5 figures, J.H. advised on global/North Atlantic drivers, J.W. and S.J. analysed the glider data, M.I. ran and analysed the PWP data, G.N., B.B. and E.D. provided CTD data, A.A. analysed the OSTIA trends, J.C. and H.L. developed the UKC3 coupled capability, BG analysed wave data, V.F.L. wrote the introduction, H.L. helped running atmospheric model with different SSTs, S.M. and L.B. ran and analysed ATMostia_ens & ATMclim_ens simulations, D.C. provided CMIP6 weather regime figure, G.D. helped with atmospheric model evaluation, M.W. maintains OSTIA and provided access to it.

Competing interests

The authors declare no competing interests.

Additional information

Supplementary information The online version contains supplementary material available at <https://doi.org/10.1038/s43247-024-01413-8>.

Correspondence and requests for materials should be addressed to Ségolène Berthou.

Peer review information *Communications Earth & Environment* thanks the anonymous reviewers for their contribution to the peer review of this work. Primary Handling Editors: Alireza Bahadori and Aliénor Lavergne. A peer review file is available.

Reprints and permissions information is available at <http://www.nature.com/reprints>

Publisher’s note Springer Nature remains neutral with regard to jurisdictional claims in published maps and institutional affiliations.

Open Access This article is licensed under a Creative Commons Attribution 4.0 International License, which permits use, sharing, adaptation, distribution and reproduction in any medium or format, as long as you give appropriate credit to the original author(s) and the source, provide a link to the Creative Commons licence, and indicate if changes were made. The images or other third party material in this article are included in the article's Creative Commons licence, unless indicated otherwise in a credit line to the material. If material is not included in the article's Creative Commons licence and your intended use is not permitted by statutory regulation or exceeds the permitted use, you will need to obtain permission directly from the copyright holder. To view a copy of this licence, visit <http://creativecommons.org/licenses/by/4.0/>.

© Crown Copyright as represented by Met Office and Scottish Government, and Tim Smyth, Jeremy P. Grist, Juliane Uta Wihsgott, Sam Jones, Mark Inall, Glenn Nolan, Eoghan Daly, Vivian Fraser-Leonhardt, Joel J.-M. Hirschi 2024